




Antichiral edge states and Bogoliubov Fermi surfaces in a two-dimensional proximity-induced superconductor

Gabriel F. Rodríguez Ruiz ¹, Juan Herrera Mateos ², Leandro Tosi,³ Christoph Strunk,⁴ Carlos Balseiro,¹ and Liliana Arrachea ^{1, a}

¹*Departamento de Sólidos Cuánticos y Sistemas Desordenados, Centro Atómico Bariloche, Instituto de Nanociencia y Nanotecnología CONICET-CNEA and Instituto Balseiro (8400), San Carlos de Bariloche, Argentina.*

²*Instituto de Ciencias Físicas y Escuela de Ciencia y Tecnología, Universidad Nacional de San Martín, (1650) Buenos Aires, Argentina.*

³*Grupo de Circuitos Cuánticos Bariloche, Div. Dispositivos y Sensores, Centro Atómico Bariloche-CNEA, Instituto Balseiro and CONICET, (8400) San Carlos de Bariloche, Argentina.*

⁴*Institut für Experimentelle und Angewandte Physik, University of Regensburg, 93040 Regensburg, Germany.*

(Dated: June 25, 2025)

We show that a magnetic field parallel to the plane of a two-dimensional electron gas with Rashba spin orbit coupling in proximity to a superconductor leads to a topological phase in coexistence with a single pair of Bogoliubov Fermi surfaces. This phase hosts antichiral edge states of co-propagating Majorana fermions and are spatially localized at the opposite edges of the sample, perpendicular to the magnetic field. We discuss the characteristic signatures in the current-phase relation of a Josephson junction formed by two reservoirs in the topological phase.

Introduction. The search for Majorana zero modes as emergent excitations in solid-state devices motivated an impressive research activity aimed at realizing the topological superconducting phase. The efforts are mainly oriented to engineer hybrid platforms with ordinary s -wave superconductors in combination with spin-orbit coupling (SOC) and a time-reversal symmetry breaking mechanism, like a magnetic field, magnetic impurities or magnetic materials [1–4]. Heterostructures of semiconducting InAs and InSb, having a large g -factor and sizable spin-orbit coupling offer a natural playground in this context. Wires fabricated in these materials captured most of the theoretical [5, 6] and experimental early attention. This 1D topological phase has been also explored in engineered two-dimensional configurations [7], and prominent examples are planar Josephson junctions [8–12]. Beyond the realization of the localized Majorana modes, the study of two-dimensional superconductors with SOC and broken time-reversal symmetry is an active avenue of research [13]: other properties like the superconducting diode effect [14–17], the formation of Bogoliubov Fermi surfaces [18–27] and the realization of the Fulde–Ferrell–Larkin–Ovchinnikov state [28] are equally fascinating.

In this work we show the existence of a new topological superconducting phase in a two-dimensional (2D) electron system with SOC when a magnetic field is applied in-plane. The bulk spectrum of this phase is not fully gapped but has a structure of two Dirac-like cones and hosts antichiral Majorana modes that co-propagate along the edges perpendicular to the magnetic field. This feature is in contrast to fully gapped two-dimensional topological superconductors with broken time-reversal sym-

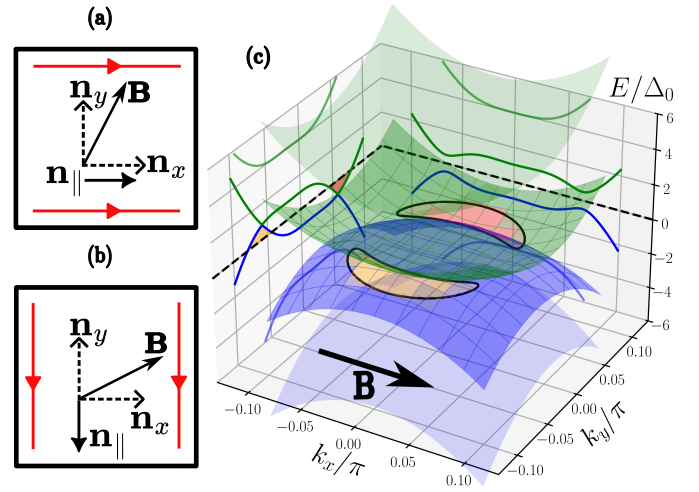


FIG. 1. Antichiral edge states: A two-dimensional electron system in proximity with an s -wave superconductor is placed in the x, y plane. The Rashba SOC is in the plane as well as the external magnetic field $\mathbf{B} = (B_x, B_y, 0)$. A topological phase with antichiral edge states along \mathbf{n}_\parallel exists for $\mu^2 \leq V^2 - \Delta_0^2$ within a range of angles satisfying $|\mathbf{n}_\parallel \cdot \mathbf{n}_V| < \Delta_0/V < 1$ (see text). (a) and (b) illustrate two different configurations of the magnetic field and the antichiral edge states. The existence of the topological phase is accompanied by the emergence of a single pair of Bogoliubov Fermi Surfaces in the spectrum. (c) BdG spectrum obtained within the lattice model for the magnetic field oriented along \mathbf{n}_x . The projected plane-cuts correspond to $(k_x = 0, k_y, E)$ and $(k_x, k_y = 0, E)$ surfaces.

metry generated by applying a magnetic field perpendicular to the plane, which has Majorana modes propagating clockwise or anticlockwise along the edges [29–32].

Topological systems with antichiral states were theoretically predicted in a modified Haldane model [33] and

^a Corresponding author: liliana.arrachea@ib.edu.ar

experimental realizations have been reported in photonic systems [34–38]. Similar co-propagating states were predicted to emerge due to the coupling between electrons and chiral phonons in graphene lattices [39, 40] and models for altermagnets[41]. In contrast to these examples, the edge modes of the two-dimensional superconducting phase we discuss in the present work are akin to lines of Majorana zero modes of stacked topological wires. This type of topological phase, where the boundary modes are present only in specific edges is identified as “weak topological phases” and have been mainly studied in the context of insulators [42] and semimetals [43]. As mentioned in these studies [42], the name does not mean lack of robustness for the edge states. We discuss the spectral properties and the topological characterization of this phase. Very interestingly, it coexists with the development of a single pair of Bogoliubov Fermi surfaces. We focus on parameters similar to those of Al/InAs heterostructures [15, 16] and discuss the experimental signatures of this phase in the current-phase relation (CPR) of Josephson junctions tailored in such 2D platform.

Model. A sketch of the system and configurations we are considering is presented in Fig. 1. We express the Hamiltonian for the 2D electron system with SOC and magnetic field in the basis $\mathbf{c}_{\mathbf{k}} = (c_{\mathbf{k},\uparrow}, c_{\mathbf{k},\downarrow})^T$. It reads $\mathcal{H}_{2D}(\mathbf{k}) = \mathbf{c}_{\mathbf{k}}^\dagger [\xi_{\mathbf{k}} + H_{\text{SOC}}(\mathbf{k}) + H_Z] \mathbf{c}_{\mathbf{k}}$, where the first term is the kinetic dispersion relation and the next terms are the SOC and Zeeman Hamiltonians,

$$H_{\text{SOC}}(\mathbf{k}) = -\mathbf{n}_z \cdot (\boldsymbol{\sigma} \times \boldsymbol{\lambda}_{\mathbf{k}}), \quad H_Z = -V \mathbf{n}_V \cdot \boldsymbol{\sigma}. \quad (1)$$

The Zeeman field is $V = \frac{1}{2}g\mu_B B$, being g the g -factor and B the strength of the magnetic field applied in the direction \mathbf{n}_V , while $\boldsymbol{\sigma}$ is the vector of Pauli matrices. In a continuum model the kinetic dispersion relation is $\xi_{\mathbf{k}} = k^2/2m - \mu$, being μ the chemical potential. We focus on Rashba SOC with $\boldsymbol{\lambda}_{\mathbf{k}} = \alpha_R(k_x, k_y, 0)$. In the calculations we also consider a square-lattice model for this system with hopping parameter t , in which case $\xi_{\mathbf{k}} = -2t(\cos k_x + \cos k_y) - \mu + 4t$ and the SOC is $\boldsymbol{\lambda}_{\mathbf{k}} = 2\lambda(\sin k_x, \sin k_y, 0)$. The proximity to the superconducting layer is modeled by a local s-wave pairing with strength Δ_0 described by the Hamiltonian

$$\mathcal{H}_{\Delta}(\mathbf{k}) = -\frac{\Delta_0}{2} \left(c_{\mathbf{k},\uparrow}^\dagger c_{-\mathbf{k},\downarrow}^\dagger + c_{-\mathbf{k},\uparrow}^\dagger c_{\mathbf{k},\downarrow}^\dagger + H.c. \right). \quad (2)$$

The ensuing Bogoliubov-de-Gennes (BdG) Hamiltonian expressed in the Nambu basis $\Psi_{\mathbf{k}} = (c_{\mathbf{k},\uparrow}, c_{\mathbf{k},\downarrow}, c_{-\mathbf{k},\downarrow}^\dagger, -c_{-\mathbf{k},\uparrow}^\dagger)^T$ reads

$$H_{\text{BdG}}(\mathbf{k}) = \frac{1}{2} [\xi_{\mathbf{k}} + H_{\text{SOC}}(\mathbf{k})] \tau^z + \frac{1}{2} H_Z - \frac{\Delta_0}{2} \tau^x, \quad (3)$$

where the Pauli matrices τ^j act on the particle-hole degree of freedom.

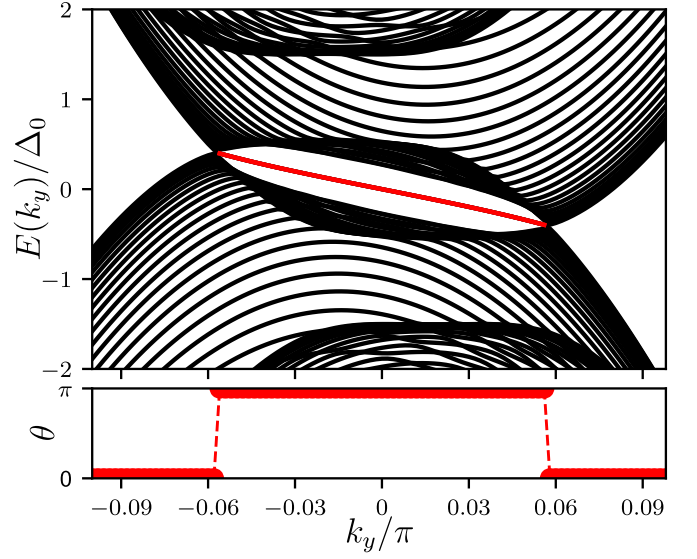


FIG. 2. **Edge states and topological invariant:** (a) Bogoliubov-de Gennes spectrum of a ribbon of $N_x = 200$ lattice sites with open boundary conditions (OBC) in x and periodic boundary conditions (PBC) along y , as a function of k_y in the topological phase for the configuration of Fig. 1(c), magnetic field along \mathbf{n}_x . The spectrum shows the dispersion relation of the edge states connecting the cones above and below the Fermi level. (b) Topological invariant $\theta(k_y)$ obtained from the numerical evaluation of the eigenvalues of the Wilson loop defined in Eq. (4) (see text). Parameters are: $t = 50\Delta_0$, $\lambda = 2.8\Delta_0$, $V = (2\Delta_0, 0, 0)$, $\mu = 0$.

A key ingredient for the topological phase we present in this work is a magnetic field with a non-vanishing projection along the direction of the SOC. We hereafter focus on a fully in-plane magnetic field, as indicated in the schemes of Fig. 1(a, b). In what follows we consider $\mathbf{n}_V \equiv \mathbf{n}_x$, which implies breaking the rotational symmetry in the plane. Hence, the spectrum has completely different features along the directions \mathbf{n}_x (parallel) and \mathbf{n}_y (perpendicular) to the magnetic field, respectively. It is important to notice that for $k_y = 0$, the spin orientation of the SOC is along \mathbf{n}_y and the Hamiltonian Eq. (3) reduces to the model of helical wires originally proposed in Refs. [5, 6]. This model has a topological phase for $\mu^2 \leq V^2 - \Delta_0^2$. Fig. 1(c) illustrates the bulk spectrum of the 2D model within this range of parameters. It can be observed that while the spectrum along k_x is gapped, along k_y two cones with a quadratic dispersion relation develop close to $k_y = 0$. They cross zero energy for larger values, leading to the formation of a single pair of Bogoliubov Fermi surfaces. These cones are asymmetric in the sense that one of them intersects the zero-energy plane from below, while the other from above.

Topological properties. The system we consider belongs to the class D of the classification presented in Ref. [44]. In fact, it has time-reversal symmetry broken while preserves particle-hole symmetry. In the case of the 1D sys-

tem corresponding to $k_y = 0$, the topological properties are defined by the value of a Berry-Zak phase and by the existence of Majorana zero modes localized at the ends of the wire. In the 2D system we study, the appropriate invariant is similar to that introduced to characterize Dirac semimetals and high-order topology [43, 45–51]. In order to obtain it, we consider periodic boundary conditions along x and y . We calculate the x -directed Wilson loop (holonomy) matrix as a function of k_y , with elements

$$\mathcal{W}^{\ell,\ell'}(k_y) = P \exp \left\{ i \int_0^{2\pi} dk_x A_{k_x}^{\ell,\ell'}(k_y) \right\}, \quad (4)$$

where P denotes path ordering, taken over the Brillouin zone of the one-dimensional Hamiltonian with fixed k_y . The Berry connection is defined as $A_{k_x}^{\ell,\ell'}(k_y) = i \langle u_{\mathbf{k}}^{\ell} | \partial_{k_x} u_{\mathbf{k}}^{\ell'} \rangle$ and it is calculated from the two lowest-energy eigenstates ℓ, ℓ' of the Hamiltonian in Eq. (3). The numerical evaluation of \mathcal{W} was done by discretizing the path as in Refs. [52, 53]. We define $\theta(k_y) = \sum_{\ell} \theta_{\ell}(k_y)$, being $\theta_{\ell}(k_y)$ the eigenvalues of the Wilson loop [43, 45–48]. In Fig. 2(b) we show the result for $\theta(k_y)$ calculated with the parameters which give the spectrum of panel (a). The energies as a function of k_y are obtained for a ribbon with $N_x = 200$ lattice sites with open boundary conditions (OBC) along x and periodic boundary conditions (PBC) along y . We can clearly identify the two cones of the bulk states, associated to the formation of a single pair of Bogoliubov Fermi surfaces, confining the range of k_y within which $\theta(k_y) = \pi$. In addition to the bulk states, we identify doubly degenerate edge states depicted in red. They are effectively described by the Hamiltonian

$$\mathcal{H}_{\text{edge}} = \sum_{\nu=l,r; k_y \geq 0} v k_y \eta_{\nu, k_y}^{\dagger} \eta_{\nu, k_y}, \quad (5)$$

where $\eta_{\nu, k_y}^{\dagger} = \eta_{\nu, -k_y}$ are Majorana modes that propagate along the y direction with the same velocity v , while they are spatially localized at the left and right ($\nu = l, r$) edges of the ribbon. Therefore, these modes are antichiral and include the Majorana zero modes $\eta_{\nu, 0}^{\dagger} = \eta_{\nu, 0}$ of the topological 1D limit. The velocity is defined by the component of the SOC perpendicular to the magnetic field and we present below an approximate expression on the basis of a low-energy Hamiltonian.

The spatial probability distribution of the lowest-positive-energy antichiral edge states is shown in Fig. 3. In both panels, the ribbon is described with OBC in x . Panel (a) shows results obtained with PBC in y , where the two edge states confined at the l and r sides of the ribbon can be clearly distinguished. Since, the previous analysis of the topological nature of the edge modes strongly relies on the existence of translational symmetry along the y direction, the question now arises on the robustness of these modes when this symmetry is broken. In panel (b) the spatial probability density

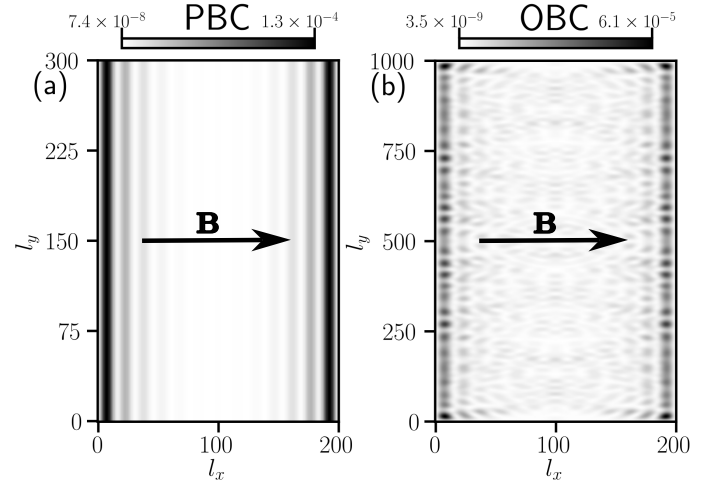


FIG. 3. **Mode localization and robustness:** Spatial probability distribution of the lowest positive energy eigenstate $E \approx 0$ within the topological phase, for a lattice with $N_x \times N_y$ sites (labeled with l_x, l_y). (a) OBC in the x -direction and PBC in the y -direction. (b) OBC are considered in both directions. In both cases $N_x = 200$ sites. In (a), $N_y^{(PBC)} = 300$, $E/t = 9.1 \times 10^{-5}$. In (b), $N_y^{(OBC)} = 1000$ and $E/t = 5.6 \times 10^{-5}$. Other parameters are the same as in Fig. 2.

is calculated with open boundary conditions in the two directions. The effect of the OBC is to introduce interference effects in the edge states mediated by the bulk states but it does not prevent their formation.

So far, we have considered a fixed orientation of the magnetic field, perpendicular to the ribbon. We would like to stress that the topological phase is not limited to this particular configuration. We recall that the $k_y = 0$ channel is equivalent to the 1D system and hence, we can rely on the boundaries of the topological phase provided in this limit by Refs. [54–58] for arbitrary orientations of the magnetic field. The result is

$$|\mathbf{n}_{||} \cdot \mathbf{n}_V| < \Delta_0/V < 1, \quad (6)$$

where $\mathbf{n}_{||}$ is the orientation of the edge that hosts the antichiral modes.

Effective low-energy model. The topological properties, including the nature of the edge states, can be better understood in terms of a low-energy effective Hamiltonian. This can be derived from the original one in Eq. (3) as explained in the Supplementary Material[59]. The result is

$$H_{\text{BdG}}^{\text{eff}}(\mathbf{k}) = d^0(\mathbf{k})\tau^0 + H^C(\mathbf{k}), \quad (7)$$

with $d^0(\mathbf{k}) = -\alpha_R k_y \xi_{\mathbf{k}}/E_{\mathbf{k}}$, $E_{\mathbf{k}} = \sqrt{\xi_{\mathbf{k}}^2 + \Delta_0^2}$ and

$$H^C(\mathbf{k}) = M(\mathbf{k})\tau^x + \Delta_x k_x \tau^y, \quad (8)$$

being $M(\mathbf{k}) = (V - E_{\mathbf{k}})$, and $\Delta_x = \alpha_R \Delta_0/(2E_{\mathbf{k}})$. This representation makes explicit the chiral symmetry $\mathcal{C} \equiv \tau^z$

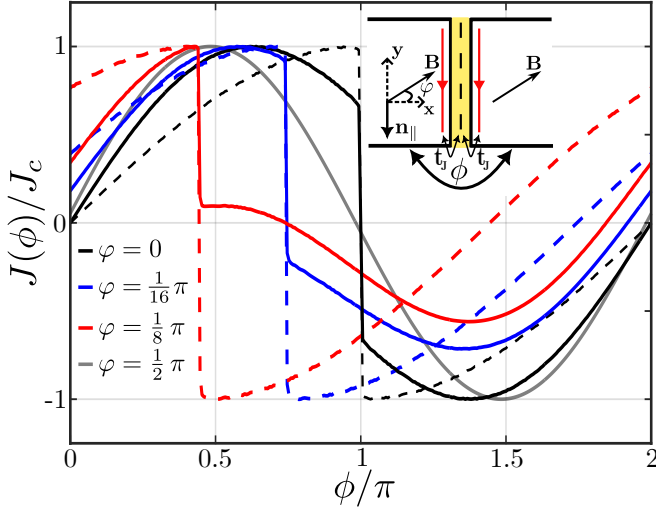


FIG. 4. **Josephson junction:** Current-phase relation (CPR) $J(\phi)$ relative to the critical current J_c at zero temperature for different magnetic field orientations on the plane with polar angle φ (see inset). The two superconductors are modeled by the lattice model with the same parameters as in Fig. 2. The junction has 200 k_y channels connected through a row of sites with a tunneling element $t_J = t/2$ (see Ref. [59]). The contribution to the CPR arising from the transverse mode with $k_y = 0$ is shown with dashed lines.

of the Hamiltonian $H_{\mathbf{k}}^C$, according to which $\mathcal{C}H^C(\mathbf{k})\mathcal{C}^{-1} = -H^C(\mathbf{k})$. Regarding k_y as a parameter, we see that the topological phase of the 1D limit ($k_y = 0$) extends over a range of values k_y satisfying $M(0, k_y) \geq 0$. We notice that Eq. (S9) is a Jackiw-Rebbi model [60, 61], with an effective mass $M(x, k_y)$. This model has zero modes at the boundaries if a domain-wall profile is assumed in the x -boundary for the mass term. Furthermore, in Ref. [59] we explicitly calculate these edge modes and verify their Majorana nature. The extra term of $H_{\text{BdG}}^{\text{eff}}(\mathbf{k})$ is proportional to τ^0 and we can express in the boundary $d^0(\mathbf{k}) = vk_y$ with $v \simeq -\alpha_R$. Hence, the eigenstates of the effective Hamiltonian in the boundary are those of $H^C(\mathbf{k})$ with the energies shifted by vk_y as stated in Eq. (5).

Josephson current. As already discussed in many works, in particular in Refs. [5, 6, 62, 63], the existence of Majorana zero modes in 1D systems generates a peculiar behavior of the current-phase relation (CPR) $J(\phi)$ in Josephson junctions. Namely, because of the 4π -periodicity of the Andreev spectrum, when Majorana zero modes hybridize at the junction, two of these states cross and $J(\phi)$ has a jump at the value of ϕ where the crossing takes place. For magnetic fields perpendicular to the SOC, this happens at $\phi = \pi$. For other orientations, the level crossing, hence the jump in the CPR, occurs at different values of ϕ [57, 64, 65].

In Josephson junctions of fully gapped 2D topological superconductors with many channels, the hybridization

of the propagating Majorana modes can be described by an effective Dirac Hamiltonian with a ϕ -dependent mass. The Andreev levels associated to the hybridization of these states with a tunneling amplitude \mathcal{T}_J have energies $\varepsilon_{k_y}(\phi) = \pm\sqrt{(vk_y)^2 + \mathcal{T}_J^2 \cos^2(\phi/2)}$ [66]. The corresponding contribution to the CPR has a jump at $k_y = 0$ as in the case of 1D systems, while the other edge-channels have a smooth non-sinusoidal behavior. In contrast, the other k_y channels (those not corresponding to the propagating edge states, i.e. the bulk modes) have a dispersion relation of the form $\varepsilon_{k_y}(\phi) = \pm E_{J,k_y} \cos(\phi)$, being E_{J,k_y} a characteristic Josephson energy. This is similar to non-topological superconductors and contributes to the CPR as $\propto \sin(\phi)$. The total $J(\phi)$, results from the contribution of all the Andreev states with negative energy. Therefore, the overall shape and features of the CPR are determined by the relative spectral weight of the edge modes among the transverse channels, and by the degree of their hybridization compared to the transparency for the bulk states.

The behavior of the CPR in the topological superconductor with antichiral Majorana modes is illustrated in Fig. 4. The configuration is shown in the inset and details on the calculations are presented in Ref. [59]. The function $J(\phi)$ relative to the critical current for 200 k_y -channels is shown for different angles φ between \mathbf{n}_x and \mathbf{n}_V . The supercurrent contribution associated to the zero mode $k_y = 0$ is shown in dashed lines, where we can clearly identify the jump at $\phi = \pi$ when $\varphi = 0$. We see that for $\varphi \neq 0$, while satisfying the condition of Eq. (6), the discontinuity in the supercurrent contribution corresponding to $k_y = 0$ is shifted to $\phi \neq \pi$. Taking into account the other k_y -channels, the impact of the zero mode is also visible within the 2D topological phase. For orientations φ beyond the condition of Eq. (6) for the boundary of the topological phase, the response is sinusoidal for all the modes as in a non-topological superconductor (grey curve). In all the cases, a response with $J(\phi = 0) \neq 0$ is observed for $\varphi \neq 0$, typical of the anomalous Josephson effect. The amplitude of the critical current is also different for different signs of ϕ , which is the characteristic feature of the superconducting diode effect [15, 16]. Similar behavior has been discussed in the framework of 1D topological superconductors [57, 65].

Conclusions. We have shown the existence of a new topological phase in a 2D proximity-induced superconductor with Rashba spin-orbit coupling. This phase develops when a magnetic field is applied in-plane and is characterized by antichiral Majorana modes propagating along the edges perpendicular to the magnetic field. This phase takes place for a range of parameters (chemical potential and magnetic field) where the Bogoliubov-de Gennes spectrum has a single pair of Bogoliubov Fermi surfaces. We have shown that signatures of these modes can be identified in the behavior of the current-phase relation of a wide Josephson junction with the edges states

oriented as sketched in Fig. 4. The topological phase persists for a range of angles close to this configuration.

The experimental realization of this phase is possible in various material platforms. It could be explored in hybrid superconductor/semiconductor heterostructures if a strategy is developed to control the chemical potential of the 2DEG. This could be realized using two quantum wells, one of them buried deep in the heterostructure to be used as a back-gate and the other one very shallow to be proximitized by the thin superconducting film. For Al/InAs heterostructures, for example, high-transparency Josephson junctions have been demonstrated, exhibiting anomalous Josephson effect and diode effect, while supporting large in-plane magnetic fields ($\sim 1.5\text{T}$) [15, 16]. The gate tunability would allow to study the progressive effect of the emergence of pairs of Bogoliubov Fermi Surfaces at reasonable fields until the conditions for the topological phase are reached. Another potential platform is a two-dimensional magnetic topological insulator like that studied in Ref. [28].

Acknowledgements: We thank Simon Feyrer, Nicola Paradiso, Luis Foa Torres, Jorge Facio, Gerardo Ortiz and Shinsei Ryu for useful discussions. We acknowledge support from CONICET and FONCyT through PICT 2020-A-03661, Argentina. L.T. acknowledges the Georg Forster Fellowship from the Alexander von Humboldt Stiftung, Germany.

-
- [1] J. Alicea, *Rep. Prog. Phys.* **75**, 076501 (2012).
 - [2] E. Prada, P. San-Jose, M. W. A. de Moor, A. Geresdi, E. J. H. Lee, J. Klinovaja, D. Loss, J. Nygård, R. Aguado, and L. P. Kouwenhoven, *Nat. Rev. Phys.* **2**, 575 (2020).
 - [3] K. Flensberg, F. von Oppen, and A. Stern, *Nat. Rev. Mater.* **6**, 944 (2021).
 - [4] W. F. Schiela, P. Yu, and J. Shabani, *PRX Quantum* **5**, 030102 (2024).
 - [5] R. M. Lutchyn, J. D. Sau, and S. Das Sarma, *Phys. Rev. Lett.* **105**, 077001 (2010).
 - [6] Y. Oreg, G. Refael, and F. von Oppen, *Phys. Rev. Lett.* **105**, 177002 (2010).
 - [7] M. Kjaergaard, F. Nichele, H. J. Suominen, M. P. Nowak, M. Wimmer, A. R. Akhmerov, J. A. Folk, K. Flensberg, J. Shabani, C. J. Palmström, and C. M. Marcus, *Nat. Commun.* **7**, 1 (2016).
 - [8] F. Pientka, A. Keselman, E. Berg, A. Yacoby, A. Stern, and B. I. Halperin, *Phys. Rev. X* **7**, 021032 (2017).
 - [9] S. Hart, H. Ren, M. Kosowsky, G. Ben-Shach, P. Leubner, C. Brüne, H. Buhmann, L. W. Molenkamp, B. I. Halperin, and A. Yacoby, *Nat. Phys.* **13**, 87 (2017).
 - [10] A. Fornieri, A. M. Whiticar, F. Setiawan, E. Portolés, A. C. C. Drachmann, A. Keselman, S. Gronin, C. Thomas, T. Wang, R. Kallaher, G. C. Gardner, E. Berg, M. J. Manfra, A. Stern, C. M. Marcus, and F. Nichele, *Nature* **569**, 89 (2019).
 - [11] H. Ren, F. Pientka, S. Hart, A. T. Pierce, M. Kosowsky, L. Lunczer, R. Schlereth, B. Scharf, E. M. Hankiewicz, L. W. Molenkamp, B. I. Halperin, and A. Yacoby, *Nature* **569**, 93 (2019).
 - [12] A. Banerjee, O. Lesser, M. A. Rahman, H.-R. Wang, M.-R. Li, A. Kringhøj, A. M. Whiticar, A. C. C. Drachmann, C. Thomas, T. Wang, M. J. Manfra, E. Berg, Y. Oreg, A. Stern, and C. M. Marcus, *Phys. Rev. B* **107**, 245304 (2023).
 - [13] C. M. Moehle, C. T. Ke, Q. Wang, C. Thomas, D. Xiao, S. Karwal, M. Lodari, V. van de Kerkhof, R. Termaat, G. C. Gardner, G. Scappucci, M. J. Manfra, and S. Goswami, *Nano Lett.* **21**, 9990 (2021).
 - [14] F. Ando, Y. Miyasaka, T. Li, J. Ishizuka, T. Arakawa, Y. Shiota, T. Moriyama, Y. Yanase, and T. Ono, *Nature* **584**, 373 (2020).
 - [15] C. Baumgartner, L. Fuchs, L. Frész, S. Reinhardt, S. Gronin, G. C. Gardner, M. J. Manfra, N. Paradiso, and C. Strunk, *Phys. Rev. Lett.* **126**, 037001 (2021).
 - [16] C. Baumgartner, L. Fuchs, A. Costa, S. Reinhardt, S. Gronin, G. C. Gardner, T. Lindemann, M. J. Manfra, P. E. Faria Junior, D. Kochan, J. Fabian, N. Paradiso, and C. Strunk, *Nature Nanotechnology* **17**, 39 (2022).
 - [17] A. Banerjee, M. Geier, M. A. Rahman, C. Thomas, T. Wang, M. J. Manfra, K. Flensberg, and C. M. Marcus, *Phys. Rev. Lett.* **131**, 196301 (2023).
 - [18] D. F. Agterberg, P. M. R. Brydon, and C. Timm, *Physical Review Letters* **118**, 127001 (2017).
 - [19] C. Setty, Y. Cao, A. Kreisel, S. Bhattacharyya, and P. Hirschfeld, *Physical Review B* **102**, 064504 (2020).
 - [20] D. Shaffer, J. Kang, F. J. Burnell, and R. M. Fernandes, *Phys. Rev. B* **101**, 224503 (2020).
 - [21] P. Dutta, F. Parhizgar, and A. M. Black-Schaffer, *Phys. Rev. Res.* **3**, 033255 (2021).
 - [22] D. Phan, J. Senior, A. Ghazaryan, M. Hatefipour, W. M. Strickland, J. Shabani, M. Serbyn, and A. P. Higginbotham, *Phys. Rev. Lett.* **128**, 107701 (2022).
 - [23] S. S. Babkin, A. P. Higginbotham, and M. Serbyn, *SciPost Phys.* **16**, 115 (2024).
 - [24] J. H. Mateos, L. Tosi, A. Braggio, F. Taddei, and L. Arrachea, *Phys. Rev. B* **110**, 075415 (2024).
 - [25] A. Pal, P. Dutta, and A. Saha, *Phys. Rev. B* **110**, 245417 (2024).
 - [26] G. Cohen, R. Seshadri, M. Khodas, and D. Meidan, *Phys. Rev. B* **109**, 165427 (2024).
 - [27] R. Ohashi, S. Kobayashi, S. Kanazawa, Y. Tanaka, and Y. Kawaguchi, *Phys. Rev. B* **110**, 104515 (2024).
 - [28] P. Mandal, S. Mondal, M. P. Stehno, S. Ilić, F. S. Bergeret, T. M. Klapwijk, C. Gould, and L. W. Molenkamp, *Nat. Phys.* **20**, 984 (2024).
 - [29] J. D. Sau, R. M. Lutchyn, S. Tewari, and S. Das Sarma, *Phys. Rev. Lett.* **104**, 040502 (2010).
 - [30] J. Alicea, *Phys. Rev. B* **81**, 125318 (2010).
 - [31] B. A. Bernevig, *Topological Insulators and Topological Superconductors* (Princeton University Press, Princeton, NJ, USA, 2013).
 - [32] M. Sato and Y. Ando, *Rep. Prog. Phys.* **80**, 076501 (2017).
 - [33] E. Colomés and M. Franz, *Phys. Rev. Lett.* **120**, 086603 (2018).
 - [34] P. Zhou, G.-G. Liu, Y. Yang, Y.-H. Hu, S. Ma, H. Xue, Q. Wang, L. Deng, and B. Zhang, *Phys. Rev. Lett.* **125**, 263603 (2020).
 - [35] X. Xi, B. Yan, L. Yang, Y. Meng, Z.-X. Zhu, J.-M. Chen, Z. Wang, P. Zhou, P. P. Shum, Y. Yang, H. Chen, S. Mandal, G.-G. Liu, B. Zhang, and Z. Gao, *Nat. Commun.* **14**, 1 (2023).

- [36] M. Wang, R.-Y. Zhang, L. Zhang, D. Wang, Q. Guo, Z.-Q. Zhang, and C. T. Chan, *Phys. Rev. Lett.* **126**, 067401 (2021).
 - [37] J. Chen and Z.-Y. Li, *Phys. Rev. Lett.* **128**, 257401 (2022).
 - [38] Y. Hu, M. Tong, T. Jiang, J.-H. Jiang, H. Chen, and Y. Yang, *Nat. Commun.* **15**, 1 (2024).
 - [39] J. Medina Dueñas, H. L. Calvo, and L. E. F. Foa Torres, *Phys. Rev. Lett.* **128**, 066801 (2022).
 - [40] J. D. Mella, H. L. Calvo, and L. E. F. Foa Torres, *Nano Lett.* **23**, 11013 (2023).
 - [41] S. Sorn, *Phys. Rev. B* **111**, L161109 (2025).
 - [42] Z. Ringel, Y. E. Kraus, and A. Stern, *Phys. Rev. B* **86**, 045102 (2012).
 - [43] B. J. Wieder, Z. Wang, J. Cano, X. Dai, L. M. Schoop, B. Bradlyn, and B. A. Bernevig, *Nat. Commun.* **11**, 1 (2020).
 - [44] A. P. Schnyder, S. Ryu, A. Furusaki, and A. W. W. Ludwig, *AIP Conf. Proc.* **1134**, 10 (2009).
 - [45] L. Fidkowski, T. S. Jackson, and I. Klich, *Phys. Rev. Lett.* **107**, 036601 (2011).
 - [46] A. Alexandradinata, X. Dai, and B. A. Bernevig, *Phys. Rev. B* **89**, 155114 (2014).
 - [47] J. Cano, B. Bradlyn, Z. Wang, L. Elcoro, M. G. Vergniory, C. Felser, M. I. Aroyo, and B. A. Bernevig, *Phys. Rev. Lett.* **120**, 266401 (2018).
 - [48] B. Bradlyn, Z. Wang, J. Cano, and B. A. Bernevig, *Phys. Rev. B* **99**, 045140 (2019).
 - [49] A. Bouhon, A. M. Black-Schaffer, and R.-J. Slager, *Phys. Rev. B* **100**, 195135 (2019).
 - [50] H.-X. Wang, G.-Y. Guo, and J.-H. Jiang, *New J. Phys.* **21**, 093029 (2019).
 - [51] O. A. Awoga, J. Cayao, and A. M. Black-Schaffer, *Phys. Rev. B* **105**, 144509 (2022).
 - [52] G. Ortiz, P. Ordejón, R. M. Martin, and G. Chiappe, *Phys. Rev. B* **54**, 13515 (1996).
 - [53] D. Pérez Daroca and A. A. Aligia, *Phys. Rev. B* **104**, 115125 (2021).
 - [54] J. Osca, D. Ruiz, and L. Serra, *Phys. Rev. B* **89**, 245405 (2014).
 - [55] S. Rex and A. Sudbø, *Phys. Rev. B* **90**, 115429 (2014).
 - [56] J. Klinovaja and D. Loss, *Eur. Phys. J. B* **88**, 1 (2015).
 - [57] A. A. Aligia, D. Pérez Daroca, and L. Arrachea, *Phys. Rev. Lett.* **125**, 256801 (2020).
 - [58] L. Gruñeiro, M. Alvarado, A. L. Yeyati, and L. Arrachea, *Phys. Rev. B* **108**, 045418 (2023).
 - [59] See Supplemental Material for details on the derivation of the effective Hamiltonian, calculation of the edge states in the effective model, and details on the calculation of the Josephson current.
 - [60] R. Jackiw and C. Rebbi, *Phys. Rev. D* **13**, 3398 (1976).
 - [61] J. Goldstone and F. Wilczek, *Phys. Rev. Lett.* **47**, 986 (1981).
 - [62] H.-J. Kwon, K. Sengupta, and V. M. Yakovenko, *Eur. Phys. J. B* **37**, 349 (2004).
 - [63] F. Pientka, A. Romito, M. Duckheim, Y. Oreg, and F. von Oppen, *New J. Phys.* **15**, 025001 (2013).
 - [64] C. Spånslätt, *Phys. Rev. B* **98**, 054508 (2018).
 - [65] J. Cayao, N. Nagaosa, and Y. Tanaka, *Phys. Rev. B* **109**, L081405 (2024).
 - [66] G. F. R. Ruiz, M. A. Rampp, A. A. Aligia, J. Schmalian, and L. Arrachea, *Phys. Rev. B* **106**, 195415 (2022).
-

Supplementary Material:
**Antichiral edge states and Bogoliubov Fermi surfaces in a two-dimensional
proximity-induced superconductor**

Gabriel F. Rodríguez Ruiz¹, Juan Herrera Mateos², Leandro Tosi³,
Christoph Strunk⁴, Carlos Balseiro¹, and Liliana Arrachea¹

¹*Departamento de Sólidos Cuánticos y Sistemas Desordenados, Centro Atómico Bariloche, Instituto de Nanociencia y Nanotecnología CONICET-CNEA and Instituto Balseiro (8400), San Carlos de Bariloche, Argentina.*

²*Instituto de Ciencias Físicas y Escuela de Ciencia y Tecnología, Universidad Nacional de San Martín, (1650) Buenos Aires, Argentina.*

³*Grupo de Circuitos Cuánticos Bariloche, Div. Dispositivos y Sensores, Centro Atómico Bariloche-CNEA, Instituto Balseiro and CONICET, (8400) San Carlos de Bariloche, Argentina.*

⁴*Institut für Experimentelle und Angewandte Physik, University of Regensburg, 93040 Regensburg, Germany.*

DETAILS OF THE DERIVATION OF THE EFFECTIVE LOW-ENERGY HAMILTONIAN

We derive a low-energy Hamiltonian with a 2×2 matrix structure following two strategies.

First order in the SOC

We consider the Hamiltonian with $\alpha_R = 0$ and the quantization axis along the magnetic field. Defining the basis $\mathbf{c}_{\mathbf{k}} = (c_{\mathbf{k},+}, c_{\mathbf{k},-})^T$, with $s = \pm$ denoting the spin parallel/antiparallel to the magnetic field, the Hamiltonian reads $\mathcal{H}_0(\mathbf{k}) = \bar{\mathcal{H}}(\mathbf{k}) + \bar{\mathcal{H}}(-\mathbf{k})$, being

$$\bar{\mathcal{H}}(\mathbf{k}) = \frac{1}{2} \left[(\xi_{\mathbf{k}} - V) c_{\mathbf{k},+}^\dagger c_{\mathbf{k},+} + (\xi_{\mathbf{k}} + V) c_{-\mathbf{k},-}^\dagger c_{-\mathbf{k},-} \right] - \frac{\Delta_0}{2} \left(c_{\mathbf{k},+}^\dagger c_{-\mathbf{k},-}^\dagger + \text{h.c.} \right). \quad (\text{S1})$$

This Hamiltonian is diagonalized by the transformation

$$\begin{pmatrix} \gamma_{\mathbf{k},+} \\ \gamma_{-\mathbf{k},-}^\dagger \end{pmatrix} = \begin{pmatrix} u_{\mathbf{k}} & -v_{\mathbf{k}} \\ v_{\mathbf{k}} & u_{\mathbf{k}} \end{pmatrix} \begin{pmatrix} c_{\mathbf{k},+} \\ c_{-\mathbf{k},-}^\dagger \end{pmatrix},$$

$$\begin{pmatrix} c_{\mathbf{k},+} \\ c_{-\mathbf{k},-}^\dagger \end{pmatrix} = \begin{pmatrix} u_{\mathbf{k}} & v_{\mathbf{k}} \\ -v_{\mathbf{k}} & u_{\mathbf{k}} \end{pmatrix} \begin{pmatrix} \gamma_{\mathbf{k},+} \\ \gamma_{-\mathbf{k},-}^\dagger \end{pmatrix},$$

with

$$u_{\mathbf{k}}^2 = \frac{1}{2} \left(1 + \frac{\xi_{\mathbf{k}}}{E_{\mathbf{k}}} \right), \quad v_{\mathbf{k}}^2 = \frac{1}{2} \left(1 - \frac{\xi_{\mathbf{k}}}{E_{\mathbf{k}}} \right), \quad (\text{S2})$$

and $E_{\mathbf{k}} = \sqrt{\xi_{\mathbf{k}}^2 + \Delta_0^2}$. Substituting in Eq. (S1) we get (up to a constant)

$$\mathcal{H}_0(\mathbf{k}) = \sum_s (E_{\mathbf{k}} - sV) \left(\gamma_{\mathbf{k},s}^\dagger \gamma_{\mathbf{k},s} + \gamma_{-\mathbf{k},s}^\dagger \gamma_{-\mathbf{k},s} \right). \quad (\text{S3})$$

We now focus on $V \gg \Delta$ and project the SOC term

$$\mathcal{H}_{\text{SOC}}(\mathbf{k}) = -\frac{\alpha_R}{2} (k_y + ik_x) \left(c_{\mathbf{k}\uparrow}^\dagger c_{\mathbf{k}\downarrow} - c_{-\mathbf{k}\uparrow}^\dagger c_{-\mathbf{k}\downarrow} \right) + \text{h.c.}, \quad (\text{S4})$$

on the lowest-energy band of the Hamiltonian Eq. (S3) (corresponding to $s = +$).

Assuming the magnetic field along x ($\mathbf{V} = V\mathbf{n}_x$), this implies substituting in Eq. (S4)

$$c_{\mathbf{k},\uparrow} = \frac{1}{\sqrt{2}} (c_{\mathbf{k},+} + c_{\mathbf{k},-}) \rightarrow \frac{1}{\sqrt{2}} \left(u_{\mathbf{k}} \gamma_{\mathbf{k},+} - v_{\mathbf{k}} \gamma_{-\mathbf{k},+}^\dagger \right), \quad c_{\mathbf{k},\downarrow} = \frac{1}{\sqrt{2}} (c_{\mathbf{k},+} - c_{\mathbf{k},-}) \rightarrow \frac{1}{\sqrt{2}} \left(u_{\mathbf{k}} \gamma_{\mathbf{k},+} + v_{\mathbf{k}} \gamma_{-\mathbf{k},+}^\dagger \right). \quad (\text{S5})$$

After some algebra we get

$$\mathcal{H}_{\text{SOC}}^{\text{eff}}(\mathbf{k}) = - (u_{\mathbf{k}}^2 - v_{\mathbf{k}}^2) \alpha_R k_y \left(\gamma_{\mathbf{k},+}^\dagger \gamma_{\mathbf{k},+} - \gamma_{-\mathbf{k},+}^\dagger \gamma_{-\mathbf{k},+} \right) - i \alpha_R k_x u_{\mathbf{k}} v_{\mathbf{k}} \left(\gamma_{\mathbf{k},+}^\dagger \gamma_{-\mathbf{k},+}^\dagger - \gamma_{-\mathbf{k},+} \gamma_{\mathbf{k},+} \right). \quad (\text{S6})$$

Combining Eqs. (S3) and (S6) and expressing this Hamiltonian in the basis $\Gamma(\mathbf{k}) = \left(\gamma_{\mathbf{k},+}, \gamma_{-\mathbf{k},+}^\dagger \right)^T$ as $\mathcal{H}_{\text{eff}}(\mathbf{k}) = \Gamma^\dagger(\mathbf{k}) H_{\text{eff}}^{\text{BdG}}(\mathbf{k}) \Gamma(\mathbf{k})$, we get the following BdG Hamiltonian

$$\begin{aligned} H_{\text{BdG}}^{\text{eff}}(\mathbf{k}) &= (E_{\mathbf{k}} - V) \tau^z + d^0(\mathbf{k}) \tau^0 + \Delta_x k_x \tau^y, \\ d^0(\mathbf{k}) &= -\frac{\alpha_R \xi_{\mathbf{k}}}{E_{\mathbf{k}}} k_y, \quad \Delta_x = \frac{\alpha_R \Delta_0}{2E_{\mathbf{k}}}. \end{aligned} \quad (\text{S7})$$

Here we see that there is an induced pairing with odd momentum dependence (p-wave type) in the direction of the magnetic field. Under the transformation $U^\dagger H U$, with $U = (\tau^0 - i\tau^y)/\sqrt{2}$, this Hamiltonian can be expressed as

$$H_{\text{BdG}}^{\text{eff}}(\mathbf{k}) = H^C(\mathbf{k}) + d^0(\mathbf{k}) \tau^0, \quad (\text{S8})$$

with

$$H^C(\mathbf{k}) = M(\mathbf{k}) \tau^x + \Delta_x k_x \tau^y, \quad M(\mathbf{k}) = (V - E_{\mathbf{k}}). \quad (\text{S9})$$

Linear order in the pairing, linear order in the SOC

Another route to derive the effective Hamiltonian Eq. (S7) is to start by diagonalizing the normal part of the Hamiltonian including the kinetic, the SOC and the Zeeman fields.

Expressing the normal part of the Hamiltonian in $\mathbf{c}_{\mathbf{k}} = (c_{\mathbf{k},\uparrow}, c_{\mathbf{k},\downarrow})^T$, it reads $\mathcal{H}_{2\text{D}}(\mathbf{k}) = \mathbf{c}_{\mathbf{k}}^\dagger H_0(\mathbf{k}) \mathbf{c}_{\mathbf{k}}$, with $H_0(\mathbf{k}) = \xi_{\mathbf{k}} + H_{\text{SOC}}(\mathbf{k}) + H_Z$. It is diagonalized by the transformation

$$\begin{aligned} \begin{pmatrix} c_{\mathbf{k},+}^\dagger \\ c_{\mathbf{k},-}^\dagger \end{pmatrix} &= \frac{1}{\sqrt{2}} \begin{pmatrix} 1 & e^{i\theta_{\mathbf{k}}} \\ -e^{-i\theta_{\mathbf{k}}} & 1 \end{pmatrix} \begin{pmatrix} c_{\mathbf{k},\uparrow}^\dagger \\ c_{\mathbf{k},\downarrow}^\dagger \end{pmatrix}, \\ \begin{pmatrix} c_{\mathbf{k},\uparrow}^\dagger \\ c_{\mathbf{k},\downarrow}^\dagger \end{pmatrix} &= \frac{1}{\sqrt{2}} \begin{pmatrix} 1 & -e^{i\theta_{\mathbf{k}}} \\ e^{-i\theta_{\mathbf{k}}} & 1 \end{pmatrix} \begin{pmatrix} c_{\mathbf{k},+}^\dagger \\ c_{\mathbf{k},-}^\dagger \end{pmatrix}, \end{aligned}$$

with $\theta_{\mathbf{k}} = \tan^{-1}(B_{\mathbf{k}}^y/B_{\mathbf{k}}^x)$ and $\mathbf{B}_{\mathbf{k}} = (B_{\mathbf{k}}^x, B_{\mathbf{k}}^y, 0)$, with $B_{\mathbf{k}}^x = -V_x - \alpha_R k_y$, $B_{\mathbf{k}}^y = -V_y + \alpha_R k_x$. The result reads

$$\mathcal{H}_{2\text{D}}(\mathbf{k}) = \sum_{s=\pm} \xi_{\mathbf{k},s} c_{\mathbf{k},s}^\dagger c_{\mathbf{k},s}, \quad (\text{S10})$$

with $\xi_{\mathbf{k},\pm} = \xi_{\mathbf{k}} \pm |B_{\mathbf{k}}|$, and $|B_{\mathbf{k}}| = \sqrt{(B_{\mathbf{k}}^x)^2 + (B_{\mathbf{k}}^y)^2}$.

The pairing induced by proximity – see the Hamiltonian Eq. (2) of the main text – expressed in the transformed basis reads

$$\mathcal{H}_{\Delta}(\mathbf{k}) = \Delta_{\mathbf{k},+} c_{\mathbf{k},+}^\dagger c_{-\mathbf{k},+}^\dagger + \Delta_{\mathbf{k},-} c_{\mathbf{k},-}^\dagger c_{-\mathbf{k},-}^\dagger + \Delta'_{\mathbf{k}} c_{\mathbf{k},+}^\dagger c_{-\mathbf{k},-}^\dagger - (\Delta'_{\mathbf{k}})^* c_{\mathbf{k},-}^\dagger c_{-\mathbf{k},+}^\dagger + \text{h.c.}, \quad (\text{S11})$$

with

$$\begin{aligned} \Delta_{\mathbf{k},+} &= -\Delta_0 (e^{-i\theta_{-\mathbf{k}}} - e^{-i\theta_{\mathbf{k}}})/4 = -\Delta_0 (\cos \theta_{-\mathbf{k}} - \cos \theta_{\mathbf{k}} + i \sin \theta_{\mathbf{k}} - i \sin \theta_{-\mathbf{k}})/4, \\ \Delta_{\mathbf{k},-} &= -\Delta_0 (e^{i\theta_{-\mathbf{k}}} - e^{i\theta_{\mathbf{k}}})/4 = -\Delta_0 (\cos \theta_{-\mathbf{k}} - \cos \theta_{\mathbf{k}} + i \sin \theta_{-\mathbf{k}} - i \sin \theta_{\mathbf{k}})/4, \\ \Delta'_{\mathbf{k}} &= -\Delta_0 (1 + e^{-i\theta_{\mathbf{k}}} e^{i\theta_{-\mathbf{k}}})/4 = -\Delta_0 [1 + \cos(\theta_{\mathbf{k}} - \theta_{-\mathbf{k}}) - i \sin(\theta_{\mathbf{k}} - \theta_{-\mathbf{k}})]/4. \end{aligned} \quad (\text{S12})$$

Assuming the magnetic field along x ($\mathbf{V} = V \mathbf{n}_x$) and $V > \alpha_R |\mathbf{k}|$, we can approximate these expressions by keeping terms up to linear order in k_x/V , k_y/V as follows, $\tan(\theta_{\mathbf{k}}) \simeq -\alpha_R k_x/V$. The two pairing potentials read

$$\Delta_{\mathbf{k},s} \simeq -i \frac{s \Delta_0 \alpha_R k_x}{2V}, \quad \Delta'_{\mathbf{k}} \simeq -\frac{\Delta_0}{2} \left(1 + i \frac{\alpha_R k_x}{V} \right). \quad (\text{S13})$$

The relevant subspace for the topological phase corresponds to the lower band $s = -$ of Eq. (S10). We assume that the Fermi energy is within this band. Hence, the dominant induced pairing is $\Delta_{\mathbf{k},-}$ defined in Eq. (S11). Therefore, the effective Hamiltonian reduces to

$$\overline{\mathcal{H}}_{\text{eff}}(\mathbf{k}) \simeq (\xi_{\mathbf{k}} - V - \alpha_R k_y) c_{\mathbf{k},-}^\dagger c_{\mathbf{k},-} - \left(i \frac{\Delta_0 \alpha_R k_x}{2V} c_{\mathbf{k},-}^\dagger c_{-\mathbf{k},-}^\dagger + \text{h.c.} \right), \quad (\text{S14})$$

where we have approximated $|B_{\mathbf{k}}| \simeq V + \alpha_R k_y$. Introducing the Nambu basis $\mathbf{c}_{\mathbf{k}} = (c_{\mathbf{k},-}, c_{-\mathbf{k},-}^\dagger)^T$, we can define $\mathcal{H}_{\text{eff}}(\mathbf{k}) = [\overline{\mathcal{H}}_{\text{eff}}(\mathbf{k}) + \overline{\mathcal{H}}_{\text{eff}}(-\mathbf{k})]/2$ and express it as follows $\mathcal{H}_{\text{eff}}(\mathbf{k}) = \mathbf{c}_{\mathbf{k}}^\dagger H_{\text{BdG}}^{\text{eff}}(\mathbf{k}) \mathbf{c}_{\mathbf{k}}$, with

$$H_{\text{BdG}}^{\text{eff}}(\mathbf{k}) = (\xi_{\mathbf{k}} - V) \tau^z + \frac{\Delta_0 \alpha_R k_x}{2V} \tau^y - \alpha_R k_y \tau^0. \quad (\text{S15})$$

Recalling that the topological phase takes place for $\mu^2 \leq V^2 - \Delta_0^2$, we see that Eq. (S15) agrees with Eq. (S7) up to corrections $\propto \Delta_0^2$ within the range of parameters defining this phase.

CALCULATION OF THE EDGE STATES IN THE EFFECTIVE CONTINUUM MODEL

We now show that the Hamiltonian Eq. (S9) regarded as $H_C(x, k_y)$ has zero modes at the boundaries of the x direction, within a certain range of k_y . To this end, we study the Jackiw-Rebbi Hamiltonian resulting from linearizing $H_C(\mathbf{k})$ in k_x while keeping k_y as a parameter,

$$H_{\text{JR}}(k_y) = M(x, k_y) \tau^x - i \partial_x \Delta_x \tau^y. \quad (\text{S16})$$

We first notice that the topological phase exists for $M_0(k_y) = V - \sqrt{(\gamma k_y^2 - \mu)^2 + \Delta_0^2} \geq 0$, being $\gamma = 1/2m$. This includes the special case $k_y = 0$, where the model is equivalent to the 1D topological model for $V^2 \geq \mu^2 + \Delta_0^2$, and extends over the range of k_y satisfying

$$|k_y| \leq \frac{1}{\sqrt{\gamma}} \sqrt{\sqrt{V^2 - \Delta_0^2} + \mu}, \quad (\text{S17})$$

which corresponds to the position of the cones in the spectrum.

To analyze the existence of a zero mode at the right boundary, we consider the topological phase in $x < 0$ and assume a domain wall at $x = 0$ as follows: $M(x, k_y) = M_0(k_y) > 0$, $x < 0$, and $M(x, k_y) = M_0(k_y) < 0$, $x > 0$. We assume $\Delta_x > 0$ and look for a normalizable solution of

$$[M_0(k_y) \tau^x - i \partial_x \Delta_x \tau^y] \Psi_0(x, k_y) = 0. \quad (\text{S18})$$

The result is

$$\Psi_r(x, k_y) = C \chi_r e^{\frac{M_0(k_y)}{\Delta_x} x}, \quad (\text{S19})$$

with $\chi_r = (1, 0)^T$ and C a normalization constant. Taking into account the transformation leading to Eq. (S9) we notice that the operator associated to this spinor has the structure $\Gamma_r(k_y) = (\gamma_{k_y,+} - \gamma_{-k_y,+}^\dagger)/\sqrt{2}$. Multiplying by a phase factor, we can define the Majorana mode $\eta_{r,k_y} = i \Gamma_r(k_y) = \eta_{r,-k_y}^\dagger$.

Similarly, to analyze the existence of a zero mode at the left boundary, we consider the topological phase in $x > 0$ and assume a domain wall at $x = 0$ as follows: $M(x, k_y) < 0$, $x < 0$, and $M(x, k_y) = M_0(k_y) > 0$, $x > 0$. The result is

$$\Psi_l(x, k_y) = C \chi_l e^{-\frac{M_0(k_y)}{\Delta_x} x}, \quad (\text{S20})$$

with $\chi_l = (0, 1)^T$. As in the case of the r zero mode, this spinor defines a Majorana fermion $\eta_{l,k_y} = (\gamma_{k_y,+} + \gamma_{-k_y,+}^\dagger)/\sqrt{2} = \eta_{l,-k_y}^\dagger$.

When we take into account the term $\propto \tau^0$ in Eqs. (S8) and (S15), we see that these edge modes have finite energy $v k_y$, with $v \simeq -\alpha_R$.

DETAILS ON THE CALCULATION OF THE JOSEPHSON CURRENT

We calculate the Josephson current as a function of the flux Φ for a long junction with N_y transverse channels, using the equilibrium Green's function formalism.

The system consists of two superconductors, L and R , which are semi-infinite along the x -direction and modeled by a tight-binding Hamiltonian. The interface between the two superconductors is represented by a single site (see

sketch of Fig.4 in the main text). Periodic boundary conditions are assumed along the y direction, giving rise to N_y transverse channels labeled by k_y .

The total Hamiltonian is given by

$$\mathcal{H} = \mathcal{H}_L + \mathcal{H}_R + \mathcal{H}_J(\phi), \quad (\text{S21})$$

Where \mathcal{H}_α with $\alpha = L, R$ are the Hamiltonians for the two superconductors. Introducing the Nambu basis $\mathbf{c}_{\alpha, l_x, k_y} = (c_{\alpha, l_x, k_y, \uparrow}, c_{\alpha, l_x, k_y, \downarrow}, c_{\alpha, l_x, -k_y, \downarrow}^\dagger, -c_{\alpha, l_x, -k_y, \uparrow}^\dagger)^T$ they can be written as follows

$$\begin{aligned} \mathcal{H}_\alpha = & \frac{1}{2} \sum_{l_x=1}^{\infty} \left[\mathbf{c}_{\alpha, l_x, k_y}^\dagger \left[\tau^z (\xi_{k_y} - 2\lambda \sin k_y \sigma^x) - V \mathbf{n}_V \cdot \boldsymbol{\sigma} + \Delta_0 \tau^x \right] \mathbf{c}_{\alpha, l_x, k_y} \right. \\ & \left. + \mathbf{c}_{\alpha, l_x, k_y}^\dagger \left[\tau^z (-t - i s_\alpha \lambda \sigma^y) \right] \mathbf{c}_{\alpha, l_x+1, k_y} + \text{h.c.} \right], \end{aligned} \quad (\text{S22})$$

where j_x counts rows of sites along x , with $l_x = 1$ being the row closest to the junction and $s_R = -s_L = 1$. The other term of Eq. (S21) describes the junction. We assume it has an interface represented by a line of N_y normal sites to which the line of sites at the edge of each superconductor is connected through a hopping term t_J . This term reads

$$\mathcal{H}_J(\phi) = \sum_{k_y, \sigma} \left[t_J \left(e^{i\phi/4} c_{L,1,k_y\sigma}^\dagger d_{k_y,\sigma} + e^{i\phi/4} d_{k_y\sigma}^\dagger c_{R,1,k_y\sigma} + \text{h.c.} \right) + \xi_{d,k_y} d_{k_y,\sigma}^\dagger d_{k_y,\sigma} \right] \quad (\text{S23})$$

with $\phi = 2\pi\Phi/\Phi_0$, being Φ_0 the flux quantum and $\xi_{d,k_y} = -\mu + 4t - 2t \cos k_y$.

We introduce the Nambu basis for the interface $\mathbf{d}_{k_y} = (d_{k_y, \uparrow}, d_{k_y, \downarrow}, d_{-k_y, \downarrow}^\dagger, -d_{-k_y, \uparrow}^\dagger)^T$ and express the hopping matrix in the Bogoliubov de Gennes representation as follows

$$\hat{\tau}(\phi) = t_J \left[e^{i\phi/4} (\tau^z + \tau^0) + e^{-i\phi/4} (\tau^z - \tau^0) \right] \frac{\sigma^0}{2}. \quad (\text{S24})$$

The Josephson current is then expressed as

$$J(\phi) = \frac{e}{\hbar} \sum_{k_y} \text{Re} \left\{ \text{Tr} \left[\tau^z \sigma^0 \hat{\tau}(\phi) \mathbf{G}_{d,L}^<(k_y; t, t) \right] \right\} = \frac{e}{\hbar} \sum_{k_y} \text{Re} \left\{ \int d\varepsilon \text{Tr} \left[\tau^z \sigma^0 \hat{\tau}(\phi) \mathbf{G}_{d,L}^<(k_y, \varepsilon) \right] \right\}, \quad (\text{S25})$$

where we have introduced the lesser Green's function

$$\mathbf{G}_{d,L}^<(t, t') = -i \langle \mathbf{c}_{L,1,k_y}^\dagger(t') \mathbf{d}_{k_y}(t) \rangle, \quad (\text{S26})$$

and its Fourier transform $t - t' \rightarrow \varepsilon$. Using Langreth rules, we obtain

$$\mathbf{G}_{d,L}^<(k_y, \varepsilon) = \mathbf{G}_{d,d}^<(k_y, \varepsilon) \hat{\tau}^\dagger(\phi) \mathbf{g}_L^a(k_y, \varepsilon) + \mathbf{G}_{d,d}^r(k_y, \varepsilon) \hat{\tau}^\dagger(\phi) \mathbf{g}_L^<(k_y, \varepsilon), \quad (\text{S27})$$

where we have introduced the retarded Green's functions

$$\mathbf{G}_{d,d}^r(k_y, \varepsilon) = [\mathbf{g}_{d,d}^r(k_y, \varepsilon)^{-1} - \boldsymbol{\Sigma}_L^r(k_y, \varepsilon) - \boldsymbol{\Sigma}_R^r(k_y, \varepsilon)]^{-1}, \quad (\text{S28})$$

and

$$\mathbf{g}_{d,d}^r(k_y, \varepsilon) = [\varepsilon \tau^0 - \xi_{k_y} \tau^z]^{-1}, \quad (\text{S29})$$

The self-energies are defined as

$$\boldsymbol{\Sigma}_L^r(k_y, \varepsilon) = \hat{\tau}(\phi)^\dagger \mathbf{g}_L^r(k_y, \varepsilon) \hat{\tau}(\phi), \quad (\text{S30})$$

$$\boldsymbol{\Sigma}_R^r(k_y, \varepsilon) = \hat{\tau}(\phi) \mathbf{g}_R^r(k_y, \varepsilon) \hat{\tau}^\dagger(\phi), \quad (\text{S31})$$

being \mathbf{g}_α^r ($\alpha = L, R$) the surface Green's function of the superconductor at the site adjacent to the interface. This is computed using the same recursive algorithm as in Ref. [24, 58]. The advanced Green's functions are obtained via $\mathbf{G}_{ij}^a(k_y, \varepsilon) = [\mathbf{G}_{ji}^r(k_y, \varepsilon)]^\dagger$.

In equilibrium, the lesser Green's functions are given by:

$$\mathbf{G}_{d,d}^<(k_y, \varepsilon) = f(\varepsilon) [\mathbf{G}_{d,d}^a(k_y, \varepsilon) - \mathbf{G}_{d,d}^r(k_y, \varepsilon)], \quad (\text{S32})$$

$$\mathbf{g}_L^<(k_y, \varepsilon) = f(\varepsilon) [\mathbf{g}_L^a(k_y, \varepsilon) - \mathbf{g}_L^r(k_y, \varepsilon)], \quad (\text{S33})$$

so the Josephson current becomes

$$J(\phi) = \frac{e}{h} \sum_{k_y} \left\{ \int d\varepsilon f(\varepsilon) F_{k_y}(\varepsilon) \right\}, \quad (\text{S34})$$

with

$$F_{k_y}(\varepsilon) = \text{Re} \left\{ \text{Tr} \left[\tau^z \hat{\tau}(\phi) \left(\mathbf{G}_{d,d}^a(k_y, \varepsilon) \hat{\tau}^\dagger(\phi) \mathbf{g}_L^a(k_y, \varepsilon) + \mathbf{G}_{d,d}^r(k_y, \varepsilon) \hat{\tau}^\dagger(\phi) \mathbf{g}_L^r(k_y, \varepsilon) \right) \right] \right\}. \quad (\text{S35})$$

All calculations are carried out at zero temperature.